Prolonged disturbance of proteostasis induces cellular senescence via temporal mitochondrial dysfunction and enhanced mitochondrial biogenesis in human fibroblasts

Authors: Yasuhiro Takenaka[1,2], Ikuo Inoue[2], Takanari Nakano[3], Masaaki Ikeda[4], Yoshihiko Kakinuma[1]

Affiliations: [1]Department of Physiology, Graduate School of Medicine, Nippon Medical School, Tokyo, Japan

[2]Department of Diabetes and Endocrinology, Saitama Medical University, Saitama, Japan

[3]Department of Biochemistry, Saitama Medical University, Saitama, Japan

[4]Department of Physiology, Saitama Medical University, Saitama, Japan

Correspondence

Yasuhiro Takenaka, PhD, Department of Physiology, Graduate School of Medicine, Nippon Medical School, Sendagi, Bunkyo-ku, Tokyo 113-8602, Japan, E-mail: yasuhiro-takenaka@nms.ac.jp

Key words: aging, mitochondria, oxidative stress, proteasome, lysosome, DNA damage response

16 **Abstract**

17 **Proteolytic activities decline with age, resulting in the accumulation of aggregated proteins in**
18 **aged organisms. To investigate how disturbance of proteostasis causes cellular senescence in**
19 **proliferating cells, we developed a stress-induced premature senescence (SIPS) model, in which**
20 **normal human fibroblast MRC-5 cells were treated with either the proteasome inhibitor**
21 **MG132 or V-ATPase inhibitor bafilomycin A1 (BAFA1). After 5 days of drug treatment, cells**
22 **showed morphological and functional changes associated with aging along with DNA damage**
23 **response. Time-course studies revealed significant increase in intracellular and mitochondrial**
24 **reactive oxygen species (ROS) during and after drug treatment. We also found temporal**
25 **downregulation of mitochondrial membrane potential during drug treatment, followed by an**
26 **increase in mitochondrial mass, especially after drug treatment. Notable upregulation of**
27 **PGC-1α and TFAM proteins confirmed enhanced mitochondrial biogenesis. Furthermore, the**
28 **protein levels of SOD2 and GPx4, mitochondrial antioxidant enzymes, in the mitochondrial**
29 **fraction were specifically reduced on day 1 of the treatment. Co-treatment with rapamycin**
30 **along with MG132 or BAFA1 partially attenuated induction of SIPS by suppressing**
31 **generation of excess ROS and mitochondrial biogenesis. In conclusion, the present study**

32 **revealed that disturbance of proteostasis by the inhibitors changes the distribution of**

33 **nuclear-encoded mitochondrial antioxidant enzymes at an early period of the treatment, which**

34 **induces mitochondrial ROS and temporal mitochondrial dysfunction. ROS in turn activates**

35 **stress responses pathways, followed by PGC-1α-mediated mitochondrial biogenesis. Hence, the**

36 **excessive ROS continuously generated by increased mitochondria can cause deleterious**

37 **damage to nuclear DNA, cell cycle arrest, and eventual cellular senescence.**

38

39

40

41 **Introduction**

42 Proteolytic activities and the rate of protein turnover decline in aged animals [1, 2] and humans [3].
43 The decline of proteostasis causes intracellular accumulation of crosslinked protein aggregates [4]
44 and/or autofluorescent materials called lipofuscin [5] that are prominent markers for cellular
45 senescence. Cellular senescence is characterized by permanent cell cycle arrest, morphological
46 changes such as flattened cellular shape, increased levels of lysosome, upregulation of
47 cyclin-dependent kinase (CDK) inhibitors p16 and p21 [6], enhanced activity of mTOR pathway [7],
48 occurrence of medium levels of p53 [8], and expression of senescence associated β-galactosidase
49 (SA-β-gal) [9]. Normal human fibroblasts, cultured *in vitro*, have limited proliferative capacity,
50 which is known as the "Hayflick limit". Limited replicative potential and occurrence of replicative
51 senescence are considered to be caused by a shortened telomere that triggers a DNA damage
52 response (DDR) and eventual irreversible cell cycle arrest. On the other hand, stress-induced
53 premature senescence (SIPS) can be induced via several stressors in young proliferative cells that
54 have long and functional telomeres. Several factors have been reported to serve as inducers of SIPS,
55 including DNA damaging reagents [10], producers of reactive oxygen species (ROS), expression of
56 oncogenic genes [11], and several proteasome inhibitors.

57 MG132, a tripeptide aldehyde, is a reversible inhibitor of β1 caspase-like, β2 trypsin-like,
58 and β5 chymotrypsin-like activities of 20S proteasome. At a high dose, MG132 increases ROS
59 levels and GSH depletion in human pulmonary fibroblasts [12], Chinese hamster ovary cells [13],
60 and human leukemic cells [14], which results in cell death. When human fibroblasts, including
61 MRC-5 cells, are treated with a low dose of MG132 for a long period, irreversible growth arrest and
62 premature senescence can be observed [15-17]. This indicates that prolonged disturbance of
63 proteostasis could cause premature senescence by a stress. However, the exact mechanisms
64 underlying SIPS caused by proteasome inhibitors are unknown.

65 Mitochondria are the central organelles responsible for ATP generation as a source of
66 energy supply in eukaryotic cells. During oxidative phosphorylation (OXPHOS) in mitochondria,
67 electron transfer via an electron transport chain in complexes I and III can cause leakage of electrons
68 [18], which is considered to be the major source of intracellular superoxide, hydrogen peroxide, and
69 other downstream ROS such as hydroxyl radicals. The role of mitochondria in aging is more
70 complicated. According to the mitochondrial free radical theory of aging, cumulative damages to
71 mitochondrial DNA and proteins by ROS generated via OXPHOS hamper mitochondrial function
72 and result in more ROS production [19]. This is a vicious cycle in which ROS causes successive

73 mitochondrial damage, and mitochondrial dysfunction in turn produces more ROS, eventually
74 leading to cellular senescence. Thus, accumulation of dysfunctional mitochondria seems to be one of
75 the hallmarks in senescent cells. Moreover, increase in mitochondrial mass occurs in fibroblasts that
76 undergo replicative senescence [20], SIPS [20, 21], and oncogene-induced senescence [11]. In many
77 cases, accumulated mitochondria in senescent cells also show decreased mitochondrial membrane
78 potential, which indicates mitochondrial dysfunction and increased ROS production, although the
79 levels of mitochondrial superoxide and hydrogen peroxide increase or decrease is dependent on the
80 cause of the dysfunction [18].

81 In this study, we investigated the mechanisms underlying the induction of premature
82 senescence in young human fibroblast MRC-5 cells that show Hayflick limit at around 60 population
83 doubling level (PDL), by prolonged treatment with MG132 or bafilomycin A1 (BAFA1). BAFA1, a
84 plecomacrolide, is a specific and potent inhibitor of vacuolar-type ATPases (V-ATPases), a proton
85 pump that acidifies lysosomes, which subsequently inhibit lysosomal degradation of biomolecules
86 from several clearance pathways, including macroautophagy and mitophagy [22]. In the current
87 study, both MG132 and BAFA1 impaired cellular proteostasis and induced premature senescence in
88 MRC-5 cells in a similar manner, although the target molecules of the two drugs are different. To

89 elucidate the exact mechanisms of SIPS by these drugs, we performed time-course studies on
90 senescence-associated markers, ROS, DDR, and mitochondrial function and biogenesis during and
91 after treatment with MG132 and BAFA1. We demonstrated that the initial loss of mitochondrial
92 functions is possibly caused by temporal depletion of mitochondrial antioxidant proteins and
93 sequential increase in mitochondrial ROS, which in turn could induce mitochondrial biogenesis,
94 excess production of intracellular ROS, DDR, and eventual cellular senescence.
95
96 **Results**
97 **Prolonged disturbance of proteostasis by MG132 or BAFA1 induces cell cycle arrest, DNA**
98 **damage response, and SIPS in early passage human fibroblasts**
99 To elucidate how prolonged inhibition of proteostasis induces premature senescence in fibroblasts,
100 we first established a MG132- or BAFA1-induced cellular senescence model. We exposed normal
101 human fibroblast MRC-5 cells (36-39 PDL) to low concentration of MG132 (0.1 μM) or BAFA1 (4
102 nM) for 3 or 5 days (Fig. 1A). During MG132 or BAFA1 treatment for 5 consecutive days, the cells
103 almost stopped proliferation and acquired thin needle-like morphology (Fig. S1A, day 3). When the
104 culture medium was returned to the regular medium without the inhibitor (Fig. 1A), sustained

105 growth arrest was observed (Fig. 1B). After drug removal, the cells gradually changed in
106 morphology, that is, to enlarged flat shape at around 3-4 post-treatment days (PD)(Fig. S1A, PD5),
107 which generally occurs during senescence. However, when cells were treated with the same
108 concentration of MG132 or BAFA1 for 3 consecutive days, proliferation was resumed after drug
109 removal (Fig. 1B). Induction of SIPS was also evaluated by conventional SA-β-gal staining and
110 cell-based microplate assay using SPiDER-βGal, a fluorogenic substrate for β-galactosidase. In cells
111 treated with either of the drugs for 5 consecutive days, SA-β-gal-positive cells were clearly observed
112 at PD7; whereas no such cells were observed when treated for 3 days (Fig. 1C). Therefore, we
113 performed a 5-day treatment with either of the drugs for all the experiments discussed further in this
114 report. Cell-based assay for SA-β-gal activity confirmed significant increase in the activity in cells at
115 PD3 and PD6 after treatment with MG132 (Fig. 1D, left) and BAFA1 (Fig. 1D, right) for 5 days. We
116 also observed remarkable increase in aggresome-like inclusion bodies that were morphologically
117 similar to those in cells undergoing replicative senescence (58 PDL) as early as day 1 of treatment
118 with MG132 or BAFA1 (Fig. 1E). The aggregates were detectable even at PD6.

119 Further, we investigated the induction of DDR by monitoring the expression of activated
120 H2AX (γH2A.X) during and after treatment of MG132 or BAFA1. DNA damage foci were

121 observed in nuclei of cells at PD5 (Fig. 1F). In immunoblot analyses, protein levels of γH2A.X were

122 relatively repressed during treatment but increased after the drug removal in both drug-treated cells

123 (Fig. 1G). We also performed time-course analyses of senescence-associated marker proteins. CDK

124 inhibitor p21 levels were increased as early as day 1 and remained predominantly the same thereafter,

125 indicating prompt and sustained cell cycle arrest (Fig. 1G). Prolonged and low-level expression of

126 p53, which is one of the hallmarks of cellular senescence [8], was also detected during and after drug

127 treatments. The p21 and p53 levels were comparable to control MRC-5 cells that underwent

128 replicative senescence (Fig. S1B, 55 and 60 PDL). Sustained activation of mTOR has been reported

129 to be required for cellular senescence [23, 24]. Phosphorylated ribosomal protein S6 (p-S6), a target

130 of mTORC1, depleted once during drug treatment, but recovered to the initial level (control) after

131 the treatment (Fig. 1G), indicating restoration of the growth signal in cells that ceased to proliferate

132 (Fig. 1B). Both NRF1 and NRF2, NF-E2-related factor 1 and 2 respectively, were transiently

133 upregulated at a very early period of MG132 treatment (Fig. 1H), but depleted thereafter (Fig. S2A).

134 In BAFA1-treated cells, very weak induction of NRF1 and NRF2 at 48 hrs was observed (Fig. 1I).

135 We also investigated metabolic remodeling as seen in some senescent cells, which showed

136 upregulation of both OXPHOS and glycolysis [25]. The protein levels of glucose transporter GLUT1

137 and HIF-1α that induces several glycolytic proteins did not increase in MG132- and BAFA1-treated

138 cells (Fig. S2B), implying that there was no shift toward glycolysis in our SIPS model.

139 We have also tested for SIPS induction in rat H9c2 myoblasts by MG132 or BAFA1 with

140 the same treatment regimen as adopted in MRC-5 cells, which demonstrated that SIPS induction by

141 these inhibitors is not a specific feature of human fibroblasts (data not shown).

142

143 **Prolonged treatment of MG132 or BAFA1 increases intracellular ROS, H_2O_2, and**

144 **mitochondrial ROS, but not NO**

145 Treatment of cells with various doses (1-30 μM) of MG132 increases intracellular ROS [12, 26] and

146 NO production [14], but the kinetics of ROS/NO production in fibroblasts during and after longer

147 treatment with MG132 or BAFA1 is unknown. During MG132 or BAFA1 treatment, intracellular

148 H_2O_2 and hydroxyl radical ($^{\cdot}OH$) levels detected by HYDROP and OxiORANGE, respectively, did

149 not increase on day 1 but gradually increased from day 3. From PD1 to PD5, hydroxyl radical (Fig.

150 2A and 2B) and H_2O_2 (Fig. 2C and 2D) levels were still higher than that of control cells.

151 Contrastingly, NO levels detected by DAF-FM DA fluorescent dye remained largely unchanged or

152 slightly reduced during and after treatments with either drug (Fig. S3). There was no increase in

153 mRNA and protein levels of inducible NOS (data not shown), which confirmed that NO was not the

154 cause of senescence induction in MG132- and BAFA1-treated cells.

155 To reveal the involvement of mitochondria in an increased production of intracellular

156 ROS in MG132- or BAFA1-treated cells, we assessed mitochondrial ROS levels using MitoSOX

157 superoxide indicator. Mitochondrial ROS levels significantly increased in both MG132- and

158 BAFA1-treated cells as early as day 1 of the treatment and peaked at PD3 (Fig. 2E and 2F).

159

160 **Prolonged treatment of MG132 or BAFA1 enhances mitochondrial biogenesis**

161 We next investigated changes in mitochondrial mass and mitochondrial membrane potential (Δψm)

162 using MitoTracker Green FM and MitoTracker Red CM-H2Xros, respectively. In either drug-treated

163 cells, mitochondrial mass gradually increased during treatment and remained at high levels even

164 after treatment (Fig. 3A and 3C, mitochondrial mass (Mt mass)). Contrarily, the mitochondrial

165 membrane potential increased once on day 1, compared with untreated control cells, but slightly

166 decreased on days 3 and 5, and markedly increased thereafter (Fig. 3B and 3C, Δψm).

167 Mitochondrial proliferation was also confirmed by qPCR analyses of mitochondrial DNA (mtDNA)

168 copy number (Fig. 3D). Intracellular ATP were almost at basal levels during treatment, but increased

169 thereafter (Fig. 3E), which may reflect the restoration of mitochondrial membrane potential after
170 drug treatment. These results suggest temporal mitochondrial dysfunction during drug treatment but
171 accumulation of functional mitochondria, probably by mitochondrial biogenesis, thereafter.

172 We further explored how mitochondrial mass increased in MG132- or BAFA1-treated
173 cells by assessing protein expression of key factors in mitochondrial biogenesis and clearance.
174 PGC-1α, the master regulator of mitochondrial biogenesis, was upregulated temporarily from day 3
175 to PD1 with different kinetics between MG132 and BAFA1, but downregulated thereafter (Fig. 3F).
176 In contrast, TFAM, the key mitochondrial transcription activator, was consistently elevated during
177 and after treatment. Upregulation of these factors indicated enhanced mitochondrial biogenesis in
178 MG132- and BAFA1-treated cells. Furthermore, Parkin, the ubiquitin ligase that is responsible for
179 mitophagy, was largely downregulated below basal levels, indicating suppression of mitophagic flux
180 during and after treatment. We also found that AMP-activated protein kinase alpha (AMPKα) was
181 remarkably activated, especially on days 3 and 5 (Fig. 3F), which is consistent with increase in
182 intracellular ATP levels in post-treatment periods (Fig. 3E). Increase in cytochrome c oxidase
183 subunit 4 (COX4) levels also confirmed an increase in mitochondrial mass in MG132- and
184 BAFA1-treated cells.

185

186 **MG132- or BAFA1-treatment causes reduction in mitochondrial antioxidant proteins in**

187 **mitochondrial fraction during the early period of treatment**

188 Recently, mass spectrometry analysis revealed aggregation of nuclear-encoded mitochondrial

189 proteins such as respiratory chain complex subunits as an early event in MG132-treated cells [27]. In

190 our experiments, mitochondrial ROS was significantly increased in MG132- or BAFA1-treated cells

191 as early as day 1 compared with untreated control cells (Fig. 2E), implying that enhanced ROS

192 generation and/or failure to scavenge ROS occur in the mitochondria immediately after initiation of

193 drug treatment. Thus, we investigated protein levels of two mitochondrial antioxidant enzymes,

194 superoxide dismutase (SOD2) and glutathione peroxidase (GPx4), in biochemically isolated

195 mitochondrial fraction (detailed method in Fig. S4A) of MG132- or BAFA1-treated cells. On day 1,

196 SOD2 was depleted specifically in mitochondrial fraction (Fig. 4A, Mt) in either drug-treated cells

197 although the overall SOD2 level was almost constant or slightly increased compared with control

198 cells (Fig. 4A, whole). From day 3, whole and mitochondrial SOD2 levels notably increased.

199 Similarly, GPx4 in mitochondrial fraction was also depleted on day 1 and induced thereafter. We

200 also observed reduction in NDUFS3, NADH dehydrogenase ubiquinone iron-sulfur protein 3 of

201 respiratory complex 1, in mitochondrial fraction on day 1, which was in accordance with results
202 from mass spectrometry analysis and observation of Ndufs3-EGFP localization in MG132-treated
203 cells, reported in a previous study [27]. In contrast, the protein levels of Tom40 and GAPDH in
204 mitochondrial fraction remained largely unchanged in either drug-treated cells. We also observed
205 accumulation of aggregate-like particles of SOD2 in the cytoplasm of either MG132- or
206 BAFA1-treated cells on day 1 (Fig. 4B). These results suggest that antioxidant enzymes could form
207 aggregates before translocation into mitochondria, as an early event of disturbance of proteostasis,
208 which eventually reduces mitochondrial ROS-scavenging efficiency.
209
210 **Rapamycin treatment partially attenuates cellular senescence induced by MG132 or BAFA1**
211 Mitochondrial function and biogenesis are controlled by mTOR [28]. Inhibition of mTOR by
212 rapamycin, a mTORC1 inhibitor, resulted in a decrease in mitochondrial oxidative function [29],
213 mitochondrial ROS [30], and senescence induction [31-33]. To further investigate the involvement
214 of mitochondrial biogenesis in our SIPS model, we co-treated cells with rapamycin and either
215 MG132 or BAFA1. In the case of 5 days co-treatment with rapamycin and MG132 or BAFA1 from
216 day 0 (Fig. 5A, Rapa1), cells recovered proliferation potential after PD5 (Fig. 5B). In contrast, poor

217 growth was observed in cells co-treated for 2 days from day 3 and additionally treated with only
218 rapamycin for 3 days from PD1 (Fig. 5A and 5B, Rapa2). The effects of rapamycin on SIPS were
219 also confirmed by SA-β-gal activity (Fig. 5C and S5) and intracellular H_2O_2 levels (Fig. 5D and 5E)
220 in both MG132- and BAFA1-treated cells. Furthermore, an increase in mitochondrial mass, assessed
221 by MitoTracker Green, was significantly repressed by co-treatment with rapamycin and either
222 MG132 (Rapa1) or BAFA1 (Rapa1 and Rapa2) (Fig. 5F). Different profiles of proliferative potential,
223 H_2O_2 levels, and mitochondrial mass between Rapa1 and Rapa2 suggested that cellular events during
224 the early period (days 0-3) of drug treatment intensively affect the following SIPS progression. Thus,
225 we further analyzed rapamycin effect on ROS production during early period (days 1-2) of the
226 treatment. Mitochondrial ROS significantly decreased by co-treatment with rapamycin on day 1
227 (MG132) or day 2 (BAFA1) compared with cells only treated with either MG132 or BAFA1 (Fig.
228 5G). Furthermore, protein contents of SOD2 in both whole and mitochondrial fractions increased in
229 cells co-treated with rapamycin and BAFA1, whereas those of GPx4 increased in cells co-treated
230 with rapamycin and MG132 (Fig. 5H), showing an accelerated upregulation and proper translocation
231 of mitochondrial anti-oxidant enzymes by rapamycin co-treatment.

232 Further, we evaluated significance of ROS produced during the early period of treatment

233 in mitochondrial biogenesis. Cells were co-treated with *N*-acetyl-L-cysteine (NAC), a ROS
234 scavenger, and either MG132 or BAFA1 for 2 days with 3 different starting dates (Fig. 6A,
235 NAC1-3). In both MG132- and BAFA1-treated cells, co-treatment of NAC during the initial 2 days
236 (NAC1) showed the highest suppression in the increase in mitochondrial mass at PD2 (Fig. 6B),
237 implying that ROS produced during the early period (days 1-2) greatly triggered mitochondrial
238 biogenesis.
239
240 **Discussion**
241 Previous studies have shown that SIPS is induced in human fibroblasts by treatment of proteasome
242 inhibitors such as MG132 [15-17]. However, the exact mechanisms of SIPS induction by
243 proteasome inhibition have not been clarified. In this study, we found that the prolonged disturbance
244 of proteostasis by not only MG132 but also by BAFA1, an inhibitor of lysosome function, induces
245 SIPS through early temporal mitochondrial dysfunction, sequential mitochondrial biogenesis that
246 possibly enhances excess ROS production, and eventual DDR. Notably, SIPS by MG132 and
247 BAFA1 showed similar phenotypes and kinetics of senescence-associated markers, mitochondrial
248 dysfunction and biogenesis, ROS levels, and DDR, although these reagents inhibit different

249 molecules, chymotrypsin-like protease in 20S proteasome and proton pump V-ATPase on lysosome
250 membrane, respectively. This implies the presence of shared mechanisms in SIPS induced by
251 disturbance of proteostasis regardless of initial causes. Contrastingly, there are several differences
252 between the profiles of SIPS by MG132 and BAFA1. For instance, the levels of SA-β-gal activity,
253 NRF1 and NRF2 induction, and mitochondrial biogenesis are relatively low in BAFA1-treated cells.
254 In addition, the overall SIPS progression in BAFA1-treated cells seems to be slower than that
255 observed in MG132-treated cells. Therefore, we could not exclude the occurrence of drug-specific
256 induction mechanisms in our SIPS model.

257 Mitochondria are considered to be the main source of ROS generated in cells.
258 Dysfunctional mitochondria that show decreased membrane potential and excess mitochondrial ROS
259 accumulate in senescent cells [21, 34]. It has also been established that the mitochondrial mass [20,
260 35] and OXPHOS activity [25] increase during cellular senescence. Thus, mitochondrial function
261 and metabolism are the major determinants of cellular aging [19]. Based on our results, it is likely
262 that there are two phases of mitochondrial status in which mitochondrial membrane potential only
263 temporarily decreased during MG132 or BAFA1 treatment, but significantly increased thereafter
264 (Fig. 3B) along with a significant increase in mitochondrial mass (Fig. 3A and 3D) and ATP levels

265 (Fig. 3E), suggesting an increase in functional mitochondria during the latter period of SIPS
266 progression. Enhanced mitochondrial biogenesis was confirmed by notable increase in PGC-1α and
267 TFAM proteins (Fig. 3F) that were critically involved in mitochondrial biogenesis, whereas Parkin
268 (Fig. 3F) and LC3-II (Fig. 1G) were greatly downregulated, implying that mitophagic flux was
269 suppressed during enhanced mitochondrial biogenesis (day 5 to PD2). Furthermore, we observed
270 depletion of antioxidant enzymes in mitochondrial fraction (Fig. 4A) and aggresome-like inclusions
271 of SOD2 in the cytoplasm (Fig. 4B) as early as day 1, implying that nuclear-encoded antioxidant
272 proteins were insufficiently translocated into the mitochondria.

273 Rapamycin treatment partially attenuates cellular senescence induced by MG132 or
274 BAFA1 (Fig. 5B and 5C). Rapamycin treatment with MG132 or BAFA1 during days 0-5 (Rapa1)
275 significantly suppressed intracellular H_2O_2 (Fig. 5D and 5E), mitochondrial ROS production (Fig.
276 5G), and mitochondrial biogenesis (Fig. 5F) compared with cells treated with only MG132 or
277 BAFA1. The suppression of ROS by rapamycin could be partly because of enhanced upregulation of
278 overall and mitochondrial levels of SOD2 (Fig. 5H, BAFA1) and GPx4 (Fig. 5H, MG132). We also
279 found that co-treatment with NAC during days 1 and 2 (NAC1) significantly inhibited mitochondrial
280 biogenesis (Fig. 6B). Taken together, it is likely that rapamycin attenuates MG132- or

281 BAFA1-induced SIPS by repressing an initial increase in intracellular and mitochondrial ROS levels
282 and the following mitochondrial biogenesis. On the contrary, immunoblot analyses revealed that an
283 induction level of PGC-1α was not altered by co-treatment with rapamycin compared to cells
284 without rapamycin (Fig. S6). Notably, an active form of LC3, LC3-II, was not upregulated by
285 rapamycin co-treatment (Fig. S6), implying that autophagic flux for damaged mitochondrial
286 clearance does not contribute to rapamycin effect on SIPS. Thus, further investigation is required to
287 clarify the detailed molecular link between suppression of ROS and mitochondrial biogenesis by
288 rapamycin co-treatment.

289 Proteolytic activities and rate of protein turnover decline in aged organisms, which result
290 in intracellular accumulation of insoluble protein aggregates. Whether age-related accumulation of
291 protein aggregates is the determinant of cellular senescence or a characteristic product in aged cells
292 still remains controversial. What is the link between protein aggregates observed in our SIPS model
293 and cellular senescence? We found that aggregated proteins accumulated from day 1 by treatment
294 with MG132 or BAFA1 (Fig. 1E). Overloading of increased aggregates may impair another
295 proteolytic system that is not inhibited by the drug, which changes the cytosolic environment to
296 accelerate widespread protein aggregation. Although we did not completely demonstrated that

297 mitochondrial antioxidant enzymes, SOD2 and PGx4, form aggregations and are unable to
298 translocate to the mitochondria, temporal reduction of these proteins in mitochondrial fraction (Fig.
299 4A) may reflect the proteostasis stresses caused by protein aggregates. At the final stage of SIPS
300 induction, protein aggregates were still detectable even at PD6 (Fig. 1E); nevertheless, proteasome
301 activity and lysosome acidity have recovered at PD5 (data not shown), suggesting impaired protein
302 clearance in senescent cells. Thus, it is likely that aggregated proteins accumulated at the late stage
303 of senescence induction could be resistant to proteolysis by proteasome or lysosome. For the reason
304 that we did not find autofluorescent pigments in any stage of SIPS cells, the aggresome-like particles
305 that we observed might have different properties from those of lipofuscin. Artificial
306 lipofuscin-loaded human fibroblast showed aged morphology [36]. To conclude whether these
307 aggregated inclusion bodies could be a causal factor in SIPS by prolonged disturbance of
308 proteostasis or not, we are, at present, analyzing the nature of the aggregates such as protein
309 modification like carbonylation and ubiquitination, and phenotypes of these aggresome-induced
310 cells.

311 In conclusion, disturbance of proteostasis changes distribution of nuclear-encoded
312 mitochondrial antioxidant proteins at an early period of treatment, which enhances mitochondrial

313 ROS production and temporal mitochondrial dysfunction. ROS in turn activates stress responses

314 including NRF1/2 and AMPK pathways, followed by PGC-1α-mediated mitochondrial biogenesis.

315 During the mid-stage of SIPS progression, excessive ROS is continuously generated from increased

316 mitochondria, which can cause further cumulative damage to nuclear DNA and cell cycle arrest, and

317 eventually lead to cellular senescence (Fig. 7).

318

319 **Materials and methods**

320 **Reagents**

321 MG132 and BAFA1 were purchased from ChemScene (Monmouth Junction, NJ) and Sigma-Aldrich

322 (St. Louis, MO), respectively. Diaminofluorescein-FM diacetate (DAF-FM), OxiORANGE, and

323 HYDROP were from Goryo Chemical (Sapporo, Japan). *N*-Acetyl-L-cysteine was from Fujifilm

324 Wako Pure Chemical Corp (Osaka, Japan). Rapamycin was from LC Laboratories (Woburn, MA).

325

326 **Cell culture**

327 MRC-5 cells (30 PDL) were obtained from JCRB Cell Bank. Cells were maintained in EMEM

328 (Fujifilm Wako Pure Chemical Corp, Osaka, Japan) supplemented with 10% fetal bovine serum

329 (Biological Industries, Cromwell, CT) and penicillin-streptomycin (Nacalai tesque, Kyoto, Japan) at

330 37°C in a humidified atmosphere of 5% CO_2. Cells were passaged every 2 days.

331

332 **Cell growth assay**

333 For MG132 or BAFA1 treatment, we plated 1×10^4 cells a well in a 96-well clear bottom black plate,

334 allowed them to grow for 16-24 h, and then changed the culture medium to EMEM that contained

335 MG132 or BAFA1. As a pilot experiment, we assessed the viability of cells treated with MG132

336 (0.1-1 μM) or BAFA1 (2-15 nM) at several different concentrations to determine the appropriate

337 concentration of each drug. On day 5 of drug treatment, the culture medium was replaced with

338 regular EMEM that contained no drug.

339

340 **Immunoblotting and antibodies**

341 Cells cultured in 6-cm dishes were trypsinized and harvested. Cell pellets were lysed in modified

342 RIPA buffer (20 mM Tris-HCl, pH7.4, 50 mM NaCl, 0.5% Nonidet P-40, 0.05% sodium dodecyl

343 sulfate (SDS), 1 mM EDTA). Protein concentration was determined using Quick Start Bradford dye

344 (Bio-Rad, Hercules, CA). Whole cell extracts (10-15 μg) were mixed with 5×SDS sample buffer

345 containing 2-mercaptoethanol, heated at 95°C for 3 min, and then loaded onto a
346 SDS-polyacrylamide gel. Proteins were transferred to a PVDF membrane and incubated in 1%
347 Western blocking reagent (Sigma-aldrich, St. Louis, MO) at 25°C for 1 hr. The membrane was then
348 incubated overnight with antibodies diluted in 0.5% Western blocking reagent. Antibodies used in
349 this study are summarized in a supplemental file. HRP-conjugated goat anti-mouse IgG
350 (Sigma-Aldrich) or anti-rabbit IgG (GE healthcare, Piscataway, NJ) antibodies were used as the
351 secondary antibodies and detected with ECL prime reagent (GE Healthcare). The
352 chemiluminescence signal was imaged by LAS4000 (GE Healthcare).
353
354 **SA-β-gal staining and senescence assays**
355 SA-β-gal staining was performed as described previously [9]. Quantitation of SA-β-gal activity was
356 assessed using a Cellular Senescence Plate Assay Kit - SPiDER-βGal (Dojindo, Kumamoto, Japan),
357 following the manufacturer's instructions.
358
359 **Immunofluorescence**
360 For immunofluorescence analyses of γH2A.X and SOD2, cells were fixed in 4%

361 paraformaldehyde/PBS, treated with 0.5% Triton X-100/PBS for 10 min, incubated in Blocking One

362 Histo (Nacalai tesque) for 1 h, and incubated with diluted primary antibody overnight. After several

363 PBS washes, cells were incubated with a secondary antibody conjugated to DyLight 488 (Cosmo

364 Bio Co., Ltd., Tokyo, Japan) and Hoechst 33342, and observed under a fluorescence microscope

365 IX83 (Olympus, Tokyo, Japan) using appropriate filter sets.

366

367 **Measurement of ROS and NO**

368 Production of hydroxyl radical (·OH) and hypochlorous acid (HClO) was measured using

369 OxiORANGE reagent (Goryo Chemical). H_2O_2 and NO were detected by HYDROP and

370 diaminofluorescein-FM diacetate (DAF-FM DA, Goryo Chemical), respectively. Cells plated in a

371 96-well Black IsoPlate (PerkinElmer, Waltham, MA) were incubated with 0.5 μM OxiORANGE, 1

372 μM HYDROP or 1 μM DAF-FM DA diluted in EMEM containing FBS for 30 min at 37°C, and

373 then washed with 100 μl HBSS once. Fluorescence (Ex/Em = 535/595 nm for OxiORANGE,

374 485/535 nm for HYDROP and DAF-FM DA) was measured by FilterMax F5 (Molecular Devices,

375 San Jose, CA). Normalized values were obtained by dividing fluorescent intensities of HYDROP

376 and DAF-FM DA by protein concentration or dividing the fluorescent intensities of of OxiORANGE

377 by nuclear fluorescent signal stained with Hoechst 33342 (Dojindo).

378

379 **Staining of protein aggregation**

380 Protein aggregation was visualized by Proteostat Aggresome Detection Reagent (Enzo Life Science,

381 Farmingdale, NY), according to the manufacturer's protocol. For the quantitative analysis, cells

382 plated in 96-well black plates were fixed with 2% PFA, permeabilized with 0.5% Triton X-100, and

383 stained with Proteostat Aggresome Detection Reagent diluted in EMEM containing FBS at 1:2,000

384 for 30 min at 25°C, then fluorescence was measured (Ex/Em = 485/595 nm) using FilterMax F5

385 (Molecular Devices).

386

387 **Intracellular ATP assay**

388 Intracellular ATP levels were measured using "Cell" ATP Assay reagent (Toyo B-Net, Tokyo,

389 Japan). The ATP level was normalized by the DNA content in cell lysates, which was quantified by

390 SYBR Gold stain (Thermo Fisher Scientific, Waltham, MA).

391

392 **Preparation of mitochondrial fraction**

393 The procedure for isolation of mitochondrial fraction from cultured cells is as described by Clayton *et al*

394 [37] with slight modifications. The buffer volume, number of strokes, homogenizer, and pestle used were

395 optimized for 0.5-1.0 × 10^6 cells. Frozen cell pellets were resuspended in hypotonic buffer and

396 homogenized using a disposable plastic pestle (As One Corp., Osaka, Japan) with matched Safe-Lock

397 tubes (Eppendorf, Hamburg, Germany). The detailed procedure is summarized in Fig. S4A-C.

398

399 **Live cell microscopy for mitochondrial analyses**

400 For the detection of mitochondrial mass and ΔΨm, live cells were incubated with 0.5 μM

401 MitoTracker Green FM (Thermo Fisher Scientific) and 0.5 μM MitoTracker Red CM-H2Xros

402 (Thermo Fisher Scientific) with 2 μg/mL Hoechst 33342 diluted in EMEM containing FBS for 30

403 min at 37°C, and then washed with 100 μl HBSS once. For the detection of mitochondrial ROS,

404 cells were incubated with 5 μM MitoSOX Red mitochondrial superoxide indicator (Thermo Fisher

405 Scientific) in HBSS for 10 min at 37°C, washed with HBSS 3 times, and cultured in regular medium

406 for 24 h. On the next day, cells were stained with Hoechst 33342, washed with 100 μl HBSS once,

407 and observed under an all-in-one fluorescence microscope BZ-9000 (Keyence, Osaka, Japan) using

408 appropriate filter sets. Fluorescence images were analyzed and quantified using ImageJ software ver.

409 2.0.0.

410

411 **Statistical analyses**

412 We conducted one-way ANOVA followed by Tukey's multiple comparison test. Two groups were

413 compared using a non-parametric Mann-Whitney *U* test. Differences between groups with a *p* value

414 of <0.05 were considered significant. All data were analyzed using GraphPad Prism 5.0 software

415 and presented as mean ± SD of the obtained values.

416

417 **Acknowledgement**

418 We are grateful to Santa Cruz Biotechnology, Inc. (Dallas, Tx) and Cosmo Bio Co., Ltd. (Tokyo,

419 Japan) for providing sample antibodies listed in Antibodies used in this study. We would like to

420 thank Editage (www.editage.jp) for English language editing.

421

422 **AUTHOR CONTRIBUTIONS**

423 Y. T. and Y. K. designed the research and drafted the paper; Y. T. carried out experiments and

424 analyzed data; and I. I., T. N., and M. I. supported analysis of oxidative stress.

425

426 **FUNDING INFO**

427 This work was supported by a Nippon Medical School Grant-in-Aid for Medical Research 2019.

428

429 **CONFLICT OF INTEREST**

430 The authors have no conflicts of interest to declare in association with this study.

431

432 **REFERENCES**

433 1. Hayashi, T. & Goto, S. (1998) Age-related changes in the 20S and 26S proteasome activities in the

434 liver of male F344 rats, *Mech Ageing Dev*. **102**, 55-66.

435 2. Ishigami, A. & Goto, S. (1990) Age-related change in the degradation rate of ovalbumin

436 microinjected into mouse liver parenchymal cells, *Arch Biochem Biophys*. **277**, 189-95.

437 3. Hwang, J. S., Hwang, J. S., Chang, I. & Kim, S. (2007) Age-associated decrease in proteasome

438 content and activities in human dermal fibroblasts: restoration of normal level of proteasome subunits

439 reduces aging markers in fibroblasts from elderly persons, *J Gerontol A Biol Sci Med Sci*. **62**, 490-9.

440 4. Reeg, S. & Grune, T. (2015) Protein Oxidation in Aging: Does It Play a Role in Aging Progression?,

441 *Antioxid Redox Signal*. **23**, 239-55.

442 5. Hohn, A. & Grune, T. (2013) Lipofuscin: formation, effects and role of macroautophagy, *Redox Biol*.

443 **1**, 140-4.

444 6. Chang, B. D., Watanabe, K., Broude, E. V., Fang, J., Poole, J. C., Kalinichenko, T. V. & Roninson, I.

445 B. (2000) Effects of p21Waf1/Cip1/Sdi1 on cellular gene expression: implications for carcinogenesis,

446 senescence, and age-related diseases, *Proc Natl Acad Sci U S A*. **97**, 4291-6.

447 7. Hasty, P., Sharp, Z. D., Curiel, T. J. & Campisi, J. (2013) mTORC1 and p53: clash of the gods?, *Cell*

448 *Cycle*. **12**, 20-5.

449 8. Leontieva, O. V., Gudkov, A. V. & Blagosklonny, M. V. (2010) Weak p53 permits senescence

450 during cell cycle arrest, *Cell Cycle*. **9**, 4323-7.

451 9. Dimri, G., Lee, X., Basile, G., Acosta, M., Scott, G., Roskelley, C., Medrano, E., Linskens, M.,

452 Rubelj, I. & Pereira-Smith, O. (1995) A biomarker that identifies senescent human cells in culture and in

453 aging skin in vivo, *Proc Natl Acad Sci U S A*. **92**, 9363-7.

454 10. Maejima, Y., Adachi, S., Ito, H., Hirao, K. & Isobe, M. (2008) Induction of premature senescence

455 in cardiomyocytes by doxorubicin as a novel mechanism of myocardial damage, *Aging Cell*. **7**, 125-36.

456 11. Moiseeva, O., Bourdeau, V., Roux, A., Deschenes-Simard, X. & Ferbeyre, G. (2009) Mitochondrial

457 dysfunction contributes to oncogene-induced senescence, *Mol Cell Biol*. **29**, 4495-507.

458 12. Park, W. H. & Kim, S. H. (2012) MG132, a proteasome inhibitor, induces human pulmonary

459 fibroblast cell death via increasing ROS levels and GSH depletion, *Oncol Rep*. **27**, 1284-91.

460 13. Maharjan, S., Oku, M., Tsuda, M., Hoseki, J. & Sakai, Y. (2014) Mitochondrial impairment triggers

461 cytosolic oxidative stress and cell death following proteasome inhibition, *Sci Rep*. **4**, 5896.

462 14. Chao, T. H., Chang, M. Y., Su, S. J. & Su, S. H. (2014) Inducible nitric oxide synthase mediates

463 MG132 lethality in leukemic cells through mitochondrial depolarization, *Free Radic Biol Med*. **74**,

464 175-87.

465 15. Chondrogianni, N. & Gonos, E. S. (2004) Proteasome inhibition induces a senescence-like

466 phenotype in primary human fibroblasts cultures, *Biogerontology*. **5**, 55-61.

467 16. Chondrogianni, N., Stratford, F. L., Trougakos, I. P., Friguet, B., Rivett, A. J. & Gonos, E. S. (2003)

468 Central role of the proteasome in senescence and survival of human fibroblasts: induction of a

469 senescence-like phenotype upon its inhibition and resistance to stress upon its activation, *J Biol Chem*.

470 **278**, 28026-37.

471 17. Ukekawa, R., Maegawa, N., Mizutani, E., Fujii, M. & Ayusawa, D. (2004) Proteasome inhibitors

472 induce changes in chromatin structure characteristic of senescent human fibroblasts, *Biosci Biotechnol*

473 *Biochem*. **68**, 2395-7.

474 18. Brand, M. D. (2016) Mitochondrial generation of superoxide and hydrogen peroxide as the source

475 of mitochondrial redox signaling, *Free Radic Biol Med*. **100**, 14-31.

476 19. Wei, Y., Zhang, Y. J., Cai, Y. & Xu, M. H. (2015) The role of mitochondria in mTOR-regulated

477 longevity, *Biol Rev Camb Philos Soc*. **90**, 167-81.

478 20. Lee, H. C., Yin, P. H., Chi, C. W. & Wei, Y. H. (2002) Increase in mitochondrial mass in human

479 fibroblasts under oxidative stress and during replicative cell senescence, *J Biomed Sci*. **9**, 517-26.

480 21. Passos, J. F., Nelson, G., Wang, C., Richter, T., Simillion, C., Proctor, C. J., Miwa, S., Olijslagers,

481 S., Hallinan, J., Wipat, A., Saretzki, G., Rudolph, K. L., Kirkwood, T. B. & von Zglinicki, T. (2010)

482 Feedback between p21 and reactive oxygen production is necessary for cell senescence, *Mol Syst Biol*. **6**,

483 347.

484 22. Huss, M. & Wieczorek, H. (2009) Inhibitors of V-ATPases: old and new players, *J Exp Biol*. **212**,

485 341-6.

486 23. Cho, S. & Hwang, E. S. (2012) Status of mTOR activity may phenotypically differentiate

487 senescence and quiescence, *Mol Cells*. **33**, 597-604.

488 24. Blagosklonny, M. V. (2011) Cell cycle arrest is not senescence, *Aging (Albany NY)*. **3**, 94-101.

489 25. Takebayashi, S., Tanaka, H., Hino, S., Nakatsu, Y., Igata, T., Sakamoto, A., Narita, M. & Nakao, M.
490 (2015) Retinoblastoma protein promotes oxidative phosphorylation through upregulation of glycolytic
491 genes in oncogene-induced senescent cells, *Aging Cell*. **14**, 689-97.
492 26. Legesse-Miller, A., Raitman, I., Haley, E. M., Liao, A., Sun, L. L., Wang, D. J., Krishnan, N.,
493 Lemons, J. M., Suh, E. J., Johnson, E. L., Lund, B. A. & Coller, H. A. (2012) Quiescent fibroblasts are
494 protected from proteasome inhibition-mediated toxicity, *Mol Biol Cell*. **23**, 3566-81.
495 27. Rawat, S., Anusha, V., Jha, M., Sreedurgalakshmi, K. & Raychaudhuri, S. (2019) Aggregation of
496 Respiratory Complex Subunits Marks the Onset of Proteotoxicity in Proteasome Inhibited Cells, *J Mol*
497 *Biol*. **431**, 996-1015.
498 28. Morita, M., Gravel, S. P., Hulea, L., Larsson, O., Pollak, M., St-Pierre, J. & Topisirovic, I. (2015)
499 mTOR coordinates protein synthesis, mitochondrial activity and proliferation, *Cell Cycle*. **14**, 473-80.
500 29. Ramanathan, A. & Schreiber, S. L. (2009) Direct control of mitochondrial function by mTOR, *Proc*
501 *Natl Acad Sci U S A*. **106**, 22229-32.
502 30. Martinez-Cisuelo, V., Gomez, J., Garcia-Junceda, I., Naudi, A., Cabre, R., Mota-Martorell, N.,
503 Lopez-Torres, M., Gonzalez-Sanchez, M., Pamplona, R. & Barja, G. (2016) Rapamycin reverses
504 age-related increases in mitochondrial ROS production at complex I, oxidative stress, accumulation of

505 mtDNA fragments inside nuclear DNA, and lipofuscin level, and increases autophagy, in the liver of
506 middle-aged mice, *Exp Gerontol*. **83**, 130-8.
507 31. Summer, R., Shaghaghi, H., Schriner, D., Roque, W., Sales, D., Cuevas-Mora, K., Desai, V.,
508 Bhushan, A., Ramirez, M. I. & Romero, F. (2019) Activation of the mTORC1/PGC-1 axis promotes
509 mitochondrial biogenesis and induces cellular senescence in the lung epithelium, *Am J Physiol Lung Cell*
510 *Mol Physiol*. **316**, L1049-L1060.
511 32. Leontieva, O. V., Demidenko, Z. N., Gudkov, A. V. & Blagosklonny, M. V. (2011) Elimination of
512 proliferating cells unmasks the shift from senescence to quiescence caused by rapamycin, *PLoS One*. **6**,
513 e26126.
514 33. Lerner, C., Bitto, A., Pulliam, D., Nacarelli, T., Konigsberg, M., Van Remmen, H., Torres, C. &
515 Sell, C. (2013) Reduced mammalian target of rapamycin activity facilitates mitochondrial retrograde
516 signaling and increases life span in normal human fibroblasts, *Aging Cell*. **12**, 966-77.
517 34. Nacarelli, T. & Sell, C. (2017) Targeting metabolism in cellular senescence, a role for intervention,
518 *Mol Cell Endocrinol*. **455**, 83-92.
519 35. Korolchuk, V. I., Miwa, S., Carroll, B. & von Zglinicki, T. (2017) Mitochondria in Cell Senescence:
520 Is Mitophagy the Weakest Link?, *EBioMedicine*. **21**, 7-13.

521 36. Nilsson, E. & Yin, D. (1997) Preparation of artificial ceroid/lipofuscin by UV-oxidation of
522 subcellular organelles, *Mech Ageing Dev*. **99**, 61-78.
523 37. Clayton, D. A. & Shadel, G. S. (2014) Isolation of mitochondria from tissue culture cells, *Cold*
524 *Spring Harb Protoc*. **2014**, pdb prot080002.

525

526 **Figure legends**

527 **Fig. 1**

528 Prolonged disturbance of proteostasis by MG132 or BAFA1 induces premature senescence in
529 normal human fibroblasts. (A) The experimental design to induce SIPS in MRC-5 by MG132 or
530 BAFA1. MRC-5 cells (37-40 PDL) were treated with 0.1-1 μM MG132 or 2-15 nM BAFA1
531 consecutively for 3 or 5 days without medium refreshment. On day 3 or 5, the drugs were removed
532 and cells were kept in regular culture medium for additional 5 days. Day, days during the drug
533 treatment; PD, post-treatment days. (B) Cell proliferation was monitored by measuring Hoechst
534 33342 fluorescence from PD1 to PD6. Cells were treated with MG132 or BAFA1 for 3 or 5 days,
535 and then cultured in medium without the drug for 6 days (PD1-6). Values are shown as mean ± SD
536 from 4 wells of a 96-well plate. The asterisk (*) indicates $p < 0.05$ by one-way ANOVA, followed
537 by Tukey's multiple comparison test for PD1 vs. others. (C) Representative pictures of

538 SA-β-gal-positive MRC-5 cells. Cells were treated with MG132 or BAFA1 for 3 or 5 days,

539 respectively, and stained at PD7 (cytoplasmic blue precipitate). Control, untreated young (39 PDL)

540 and old (59 PDL) MRC-5 cells undergoing replicative senescence. (D) SA-β-gal activity was

541 measured using a SPiDER-βGal Cellular Senescence Plate Assay Kit. Fluorescence signal derived

542 from SA-β-gal was normalized by Hoechst 33342-stained nuclear signal. C, untreated control cells.

543 Values are shown as mean ± SD from 4 wells of a 96-well plate. The asterisk (*) indicates $p < 0.05$

544 by one-way ANOVA, followed by Tukey's multiple comparison test for control vs. treated cells. (E)

545 Representative images of accumulation of aggresome-like inclusion bodies in senescence-induced

546 MRC-5 cells. Cells were treated with MG132 or BAFA1 for 5 days, respectively, and stained with

547 Proteostat Aggresome detection reagent (red) and Hoechst 33342 (blue). Scale bar = 50 μm. (F)

548 Representative images of control and MG132- or BAFA1-treated MRC-5 cells immunostained for

549 γH2A.X (green) and Hoechst 33342 (blue). Scale bar = 50 μm. (G) Immunoblot analyses for CDK

550 inhibitor p21, p53, DNA damage response marker γH2A.X, downstream target of mTORC1 S6 and

551 phosphorylated $S6^{Thr235/236}$, autophagy marker LC3, and GAPDH from control and MG132- or

552 BAFA1-treated MRC-5 cells. (H) Immunoblot analyses for NRF1 and NRF2 from control and

553 MG132- or BAFA1-treated MRC-5 cells.

554

555 **Fig. 2**

556 Prolonged disturbance of proteostasis by MG132 or BAFA1 enhances ROS production. (A)
557 Quantitation of relative intracellular ROS levels using OxiORANGE reagent that selectively detects
558 hydroxyl radical (·OH) and hypochlorous acid (HClO). The fluorescence intensity for OxiORANGE
559 (Ex/Em = 535/595) was normalized by Hoechst 33342 intensity (Ex/Em = 340/465). Values are
560 shown as mean ± SD from 4 wells of a 96-well plate. The asterisk (*) indicates $p < 0.05$ by one-way
561 ANOVA, followed by Tukey's multiple comparison test for control vs. treated cells. (B)
562 Representative images of control and MG132- or BAFA1-treated (PD1) MRC-5 cells stained for the
563 OxiORANGE (red) and Hoechst 33342 (blue). Scale bar = 50 μm. (C) Quantitation of relative
564 intracellular H_2O_2 levels using HYDROP reagent that selectively detects H_2O_2. The fluorescence
565 intensity for HYDROP was normalized by total protein concentration. Values are shown as mean ±
566 SD from 4 wells of a 96-well plate. (D) Representative images of control and MG132- or
567 BAFA1-treated (PD1) MRC-5 cells stained for the HYDROP (green) and Hoechst 33342 (blue).
568 Scale bar = 50 μm. (E) Relative mitochondrial ROS levels were monitored using a MitoSOX Red
569 mitochondrial superoxide indicator. The fluorescence intensities for MitoSOX and Hoechst 33342

570 were quantified by image analysis. MitoSOX intensity was normalized by the number of nuclei.

571 Values are shown as mean ± SD from the measurements of 4 different images. The asterisk (*)

572 indicates $p < 0.05$ by one-way ANOVA, followed by Tukey's multiple comparison test for control

573 vs. treated cells. Values obtained from cells treated with MG132 or BAFA1 on day 1 were compared

574 with those from untreated control cells using a non-parametric Mann-Whitney *U* test. The sharp (#)

575 indicates significant difference ($p < 0.05$). (F) Representative images of control and MG132- or

576 BAFA1-treated (PD3) MRC-5 cells stained for MitoSOX (red) and Hoechst 33342 (blue).

577

578 **Fig. 3**

579 Prolonged disturbance of proteostasis by MG132 or BAFA1 induces temporal mitochondrial

580 dysfunction and sequential mitochondrial biogenesis. (A) Relative mitochondrial mass was

581 monitored using MitoTracker Green FM. The fluorescence intensities for MitoTracker Green and

582 Hoechst 33342 were quantified by image analysis. MitoTracker Green intensity was normalized by

583 the number of nuclei. Values are shown as mean ± SD from the measurements of 5 different images.

584 The asterisk (*) indicates $p < 0.05$ by one-way ANOVA, followed by Tukey's multiple comparison

585 test for control vs. treated cells. (B) Relative mitochondrial membrane potential ($\Delta\Psi m$) was

586 monitored using MitoTracker Red CM-H_2XRos. The fluorescence intensities for MitoTracker Red

587 CM-H_2XRos and Hoechst 33342 were quantified by image analysis. MitoTracker Red CM-H_2XRos

588 intensity was normalized by the number of nuclei. Values are shown as mean ± SD from the

589 measurements of 10 different images. The asterisk (*) indicates $p < 0.05$ by one-way ANOVA

590 followed by Tukey's multiple comparison test for control vs. treated cells. (C) Representative

591 images of control and MG132- or BAFA1-treated (day 5 and PD1) MRC-5 cells stained for the

592 MitoTracker Green FM (Mt mass, green), MitoTracker Red CM-H_2XRos ($\Delta\Psi$m, Red) and Hoechst

593 33342 (blue). (D) The copy number of mitochondrial DNA of control and MG132- or

594 BAFA1-treated MRC-5 cells was measured by qPCR using mtDNA-specific primers and nuclear

595 DNA-specific primers as a reference. Values are mean ± SD of results obtained from 3-4

596 independent experiments. The asterisk (*) indicates $p < 0.05$ by one-way ANOVA, followed by

597 Tukey's multiple comparison test for control vs. treated cells. (E) Intracellular ATP contents were

598 measured using a firefly luciferase. The luminescence was normalized by cellular DNA

599 concentration quantified using SYBR Gold. Values are shown as mean ± SD from 4 wells of a

600 96-well plate. The asterisk (*) indicates $p < 0.05$ by one-way ANOVA, followed by Tukey's

601 multiple comparison test for control (37 PDL) vs. treated cells. (F) Immunoblot analyses for

602 PGC-1α, TFAM, Parkin, AMPKα, phosphorylated AMPKα^{Thr172} (p-AMPKα), COX4 and GAPDH

603 from control and MG132 (left)- or BAFA1 (right)-treated MRC-5 cells.

604

605 **Fig. 4**

606 Translocation of antioxidant enzymes to mitochondria is impaired in the early period of MG132 or

607 BAFA1 treatment in MRC-5 cells. (A) Immunoblot analyses for mitochondrial antioxidant enzymes

608 SOD2 and GPx4, NDUFS3, Tom40, and GAPDH from control and MG132 (left)- or BAFA1

609 (right)-treated MRC-5 cells. Mt, mitochondrial fraction; Whole, whole cellular extract. (B)

610 Representative images of control and MG132- or BAFA1-treated MRC-5 cells on day 1

611 immunostained for SOD2 (green) and Hoechst 33342 (blue). Scale bar = 50 μm.

612

613 **Fig. 5**

614 Rapamycin attenuates cellular senescence induced by MG132 or BAFA1. (A) The experimental

615 design for co-treatment of 10 nM rapamycin with MG132 or BAFA1 in MRC-5. Rapa1, cells were

616 co-treated with rapamycin and either MG132 or BAFA1 from day 0 to day 5. Rapa2, cells were

617 co-treated with rapamycin and either MG132 or BAFA1 from day 3 to day 5, and continuously

618 cultured in regular medium containing rapamycin from day 5 to PD3. (B) Cell proliferation was

619 monitored by measuring Hoechst 33342 fluorescence from PD5 to PD10. Values are shown as mean

620 ± SD from 4 wells of a 96-well plate. (C) SA-β-gal activities of cells co-treated with rapamycin and

621 either MG132 or BAFA1 were measured on PD5 using a SPiDER-βGal Cellular Senescence Plate

622 Assay Kit. Normalized values are shown as mean ± SD from 4 wells of a 96-well plate. Values

623 obtained from cells treated with rapamycin and either MG132 or BAFA1 (Rapa1 and Rapa2) were

624 compared with those from cells treated with only MG132 or BAFA1 (-) using a non-parametric

625 Mann-Whitney *U* test. The asterisk (*) indicates significant difference ($p < 0.05$). (D, E) Intracellular

626 H_2O_2 levels of cells co-treated with rapamycin and either MG132 or BAFA1 were measured on day

627 3, day 5, and PD3 by HYDROP staining. Normalized values are shown as mean ± SD from 4 wells

628 of a 96-well plate. Two groups were compared using a non-parametric Mann-Whitney *U* test (*$p <$

629 0.05). (F) Relative mitochondrial mass of cells co-treated with rapamycin and either of MG132 or

630 BAFA1 was measured on PD1 (MG132) and PD2 (BAFA1) using MitoTracker Green FM. Values

631 are shown as mean ± SD from the measurements of 4 different images. Two groups were compared

632 using a non-parametric Mann-Whitney *U* test (*$p < 0.05$). (G) Relative mitochondrial ROS levels of

633 cells co-treated with rapamycin (+Rapa) and either of MG132 or BAFA1 were measured on day 1

634 (MG132) and day 2 (BAFA1). The MitoSOX intensity was normalized by the number of nuclei.

635 Values are shown as mean ± SD from the measurements of 4 different images. Two groups were

636 compared using a non-parametric Mann-Whitney *U* test (*$p < 0.05$). (H) Immunoblot analyses for

637 SOD2, GPx4, Tom40, and GAPDH from MG132- or BAFA1-treated cells with (+Rapa) or without

638 (-Rapa) rapamycin on day 1. Mt, mitochondrial fraction; Whole, whole cellular extract.

639

640 **Fig. 6**

641 NAC attenuates an increase in mitochondrial mass induced by MG132 or BAFA1. (A) The

642 experimental design for co-treatment of *N*-acetyl-L-cysteine (NAC) with MG132 or BAFA1 in

643 MRC-5 cells. NAC1-3, cells were co-treated with 5 mM NAC and either of MG132 or BAFA1 from

644 day 0 to day 2 (NAC1), day 2 to day 4 (NAC2), or day 5 to PD1 (NAC3, only NAC treatment during

645 day 5 to PD1). (B) Relative mitochondrial mass of cells co-treated with NAC and either MG132 or

646 BAFA1 was measured on PD1 (MG132) and PD2 (BAFA1) using MitoTracker Green FM. Values

647 are shown as mean ± SD from the measurements of 6 different images. Two groups were compared

648 using a non-parametric Mann-Whitney *U* test (*$p < 0.05$).

649

650 **Fig. 7**

651 Speculative scheme of SIPS induced by MG132 or BAFA1. Upper panel shows mitochondrial
652 events during SIPS progression induced by MG132 or BAFA1. Disturbance of proteostasis changes
653 distribution of nuclear-encoded mitochondrial proteins including antioxidant enzymes SOD2 and
654 GPx4 at a very early period of the treatment, which induces mitochondrial ROS and temporal
655 mitochondrial dysfunction. ROS in turn activates stress response pathway including NRF1 and
656 NRF2 upregulation, followed by PGC-1α-mediated mitochondrial biogenesis. During mid-stage of
657 SIPS progression, excessive ROS was continuously generated from increased mitochondria, which
658 could cause deleterious damage to nuclear DNA and cell cycle arrest, and eventually lead to cellular
659 senescence. Lower panel summarizes kinetics of cellular outcomes including levels of SA-β-gal
660 activity, DNA damage response, overall ROS, protein aggregation, and autophagic flux.

661

662

663

Figure 1

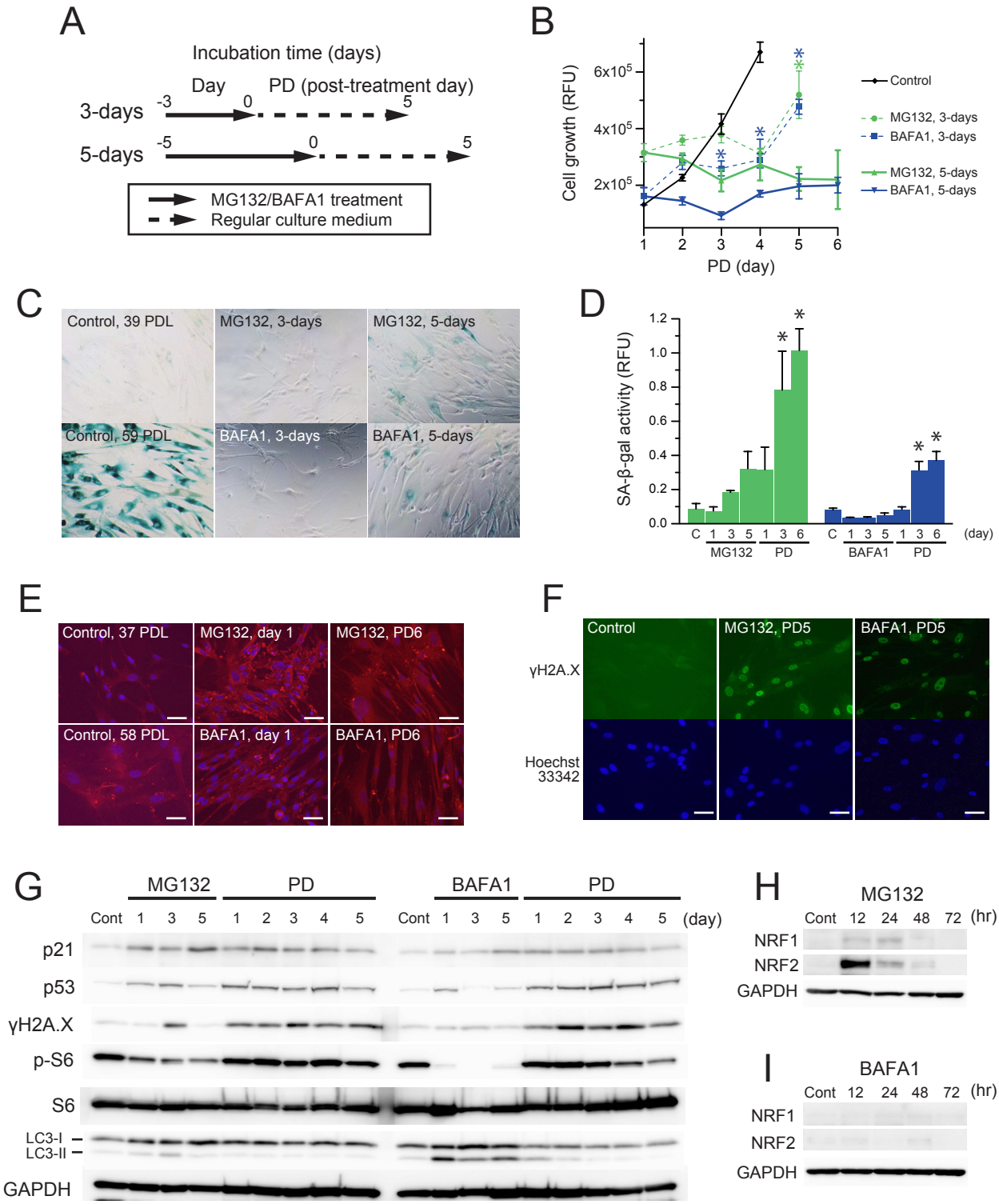
A
Incubation time (days)
Day
PD (post-treatment day)
3-days
-3
0
5
5-days
-5
0
5
MG132/BAFA1 treatment
Regular culture medium
B
Cell growth (RFU)
6x10^5
4x10^5
2x10^5
PD (day)
Control
MG132, 3-days
BAFA1, 3-days
MG132, 5-days
BAFA1, 5-days
C
Control, 39 PDL
MG132, 3-days
MG132, 5-days
Control, 59 PDL
BAFA1, 3-days
BAFA1, 5-days
D
SA-β-gal activity (RFU)
(day)
MG132
PD
BAFA1
PD
E
Control, 37 PDL
MG132, day 1
MG132, PD6
Control, 58 PDL
BAFA1, day 1
BAFA1, PD6
F
Control
MG132, PD5
BAFA1, PD5
γH2A.X
Hoechst 33342
G
MG132
PD
BAFA1
PD
Cont
(day)
p21
p53
γH2A.X
p-S6
S6
LC3-I
LC3-II
GAPDH
H
MG132
Cont
(hr)
NRF1
NRF2
GAPDH
I
BAFA1
Cont
(hr)
NRF1
NRF2
GAPDH

Figure 2

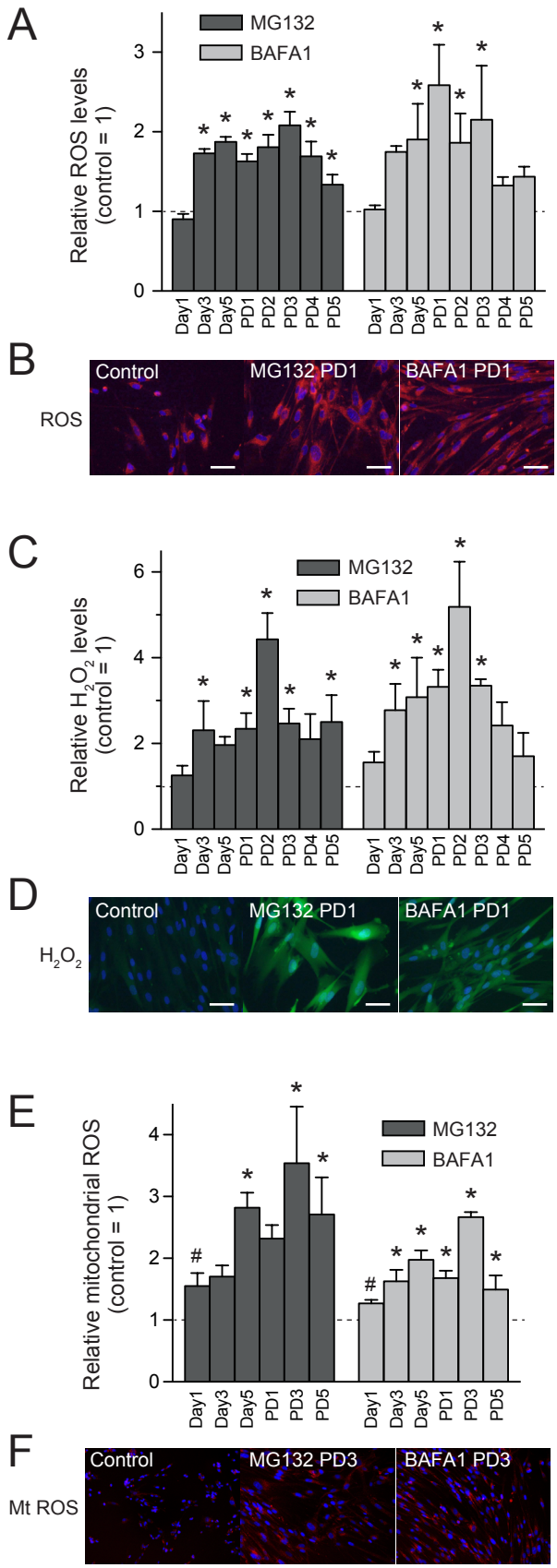
A
MG132
BAFA1
Relative ROS levels
(control = 1)
0
1
2
3
Day1
Day3
Day5
PD1
PD2
PD3
PD4
PD5
B
ROS
Control
MG132 PD1
BAFA1 PD1
C
Relative H_2O_2 levels
(control = 1)
0
2
4
6
D
H_2O_2
Control
MG132 PD1
BAFA1 PD1
E
Relative mitochondrial ROS
(control = 1)
0
1
2
3
4
F
Mt ROS
Control
MG132 PD3
BAFA1 PD3

Figure 3

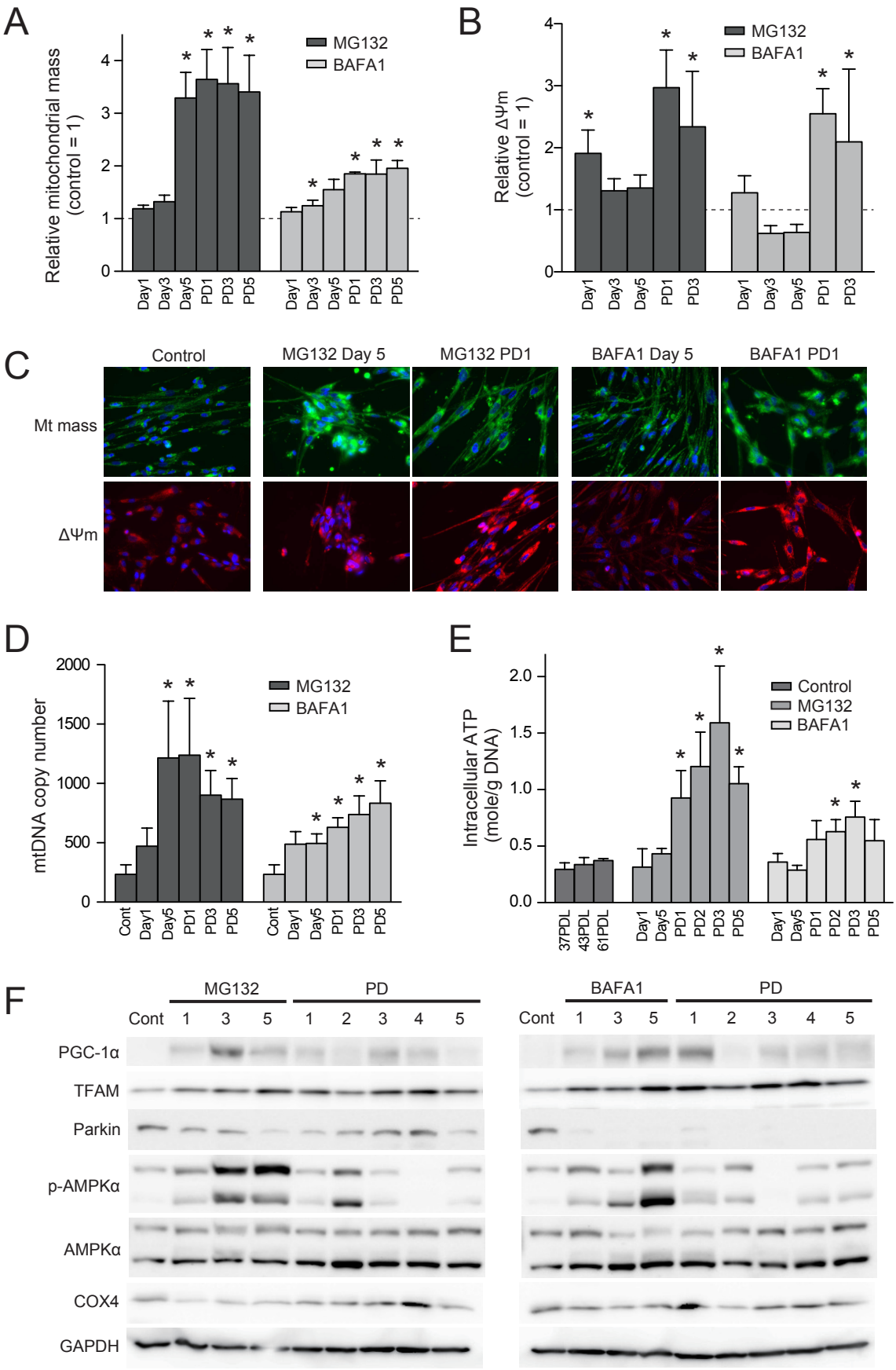
A
Relative mitochondrial mass (control = 1)
MG132
BAFA1
Day1
Day3
Day5
PD1
PD3
PD5
B
Relative ΔΨm (control = 1)
MG132
BAFA1
C
Control
MG132 Day 5
MG132 PD1
BAFA1 Day 5
BAFA1 PD1
Mt mass
ΔΨm
D
mtDNA copy number
MG132
BAFA1
Cont
E
Intracellular ATP (mole/g DNA)
Control
MG132
BAFA1
37PDL
43PDL
61PDL
PD2
F
MG132
PD
BAFA1
Cont
PGC-1α
TFAM
Parkin
p-AMPKα
AMPKα
COX4
GAPDH

Figure 4

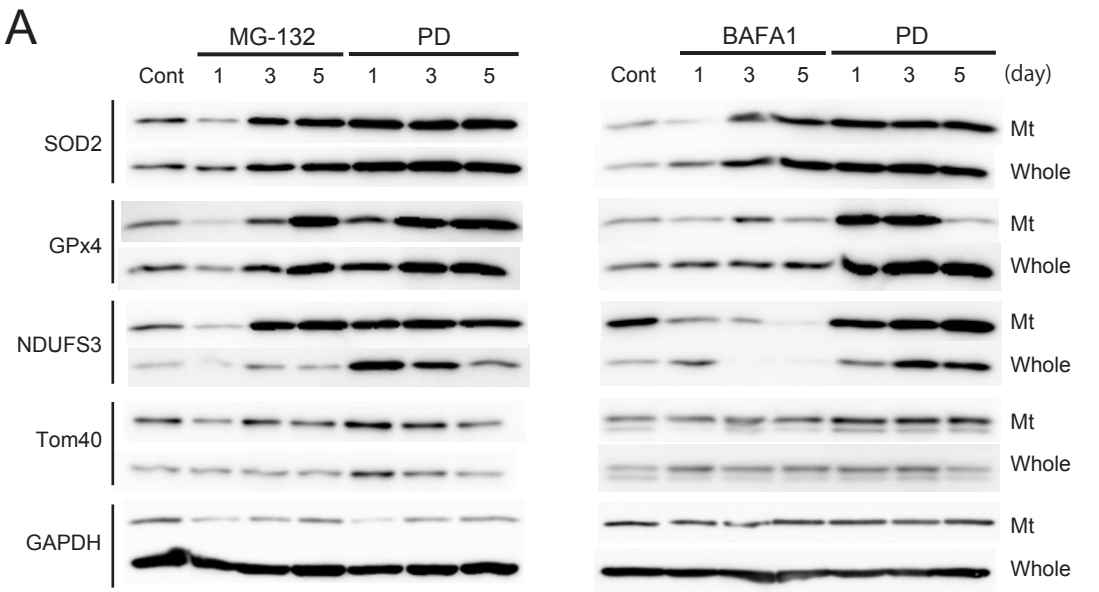
A
MG-132
PD
Cont
1
3
5
1
3
5
BAFA1
PD
Cont
1
3
5
1
3
5
(day)
SOD2
GPx4
NDUFS3
Tom40
GAPDH
Mt
Whole

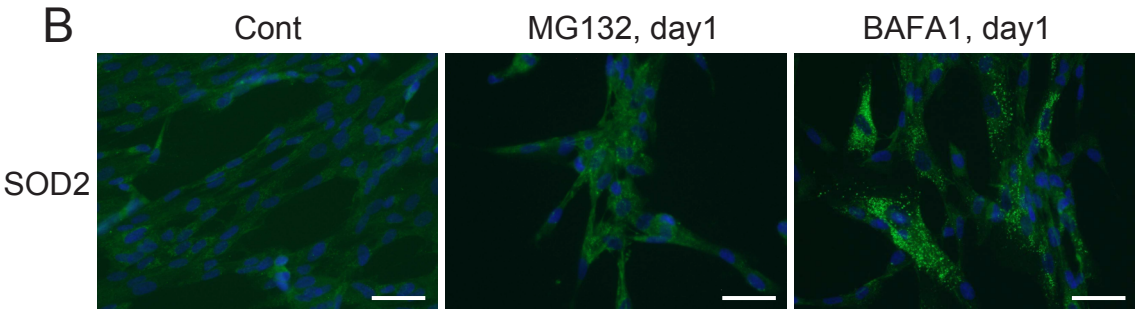
B
Cont
MG132, day1
BAFA1, day1
SOD2

Figure 5

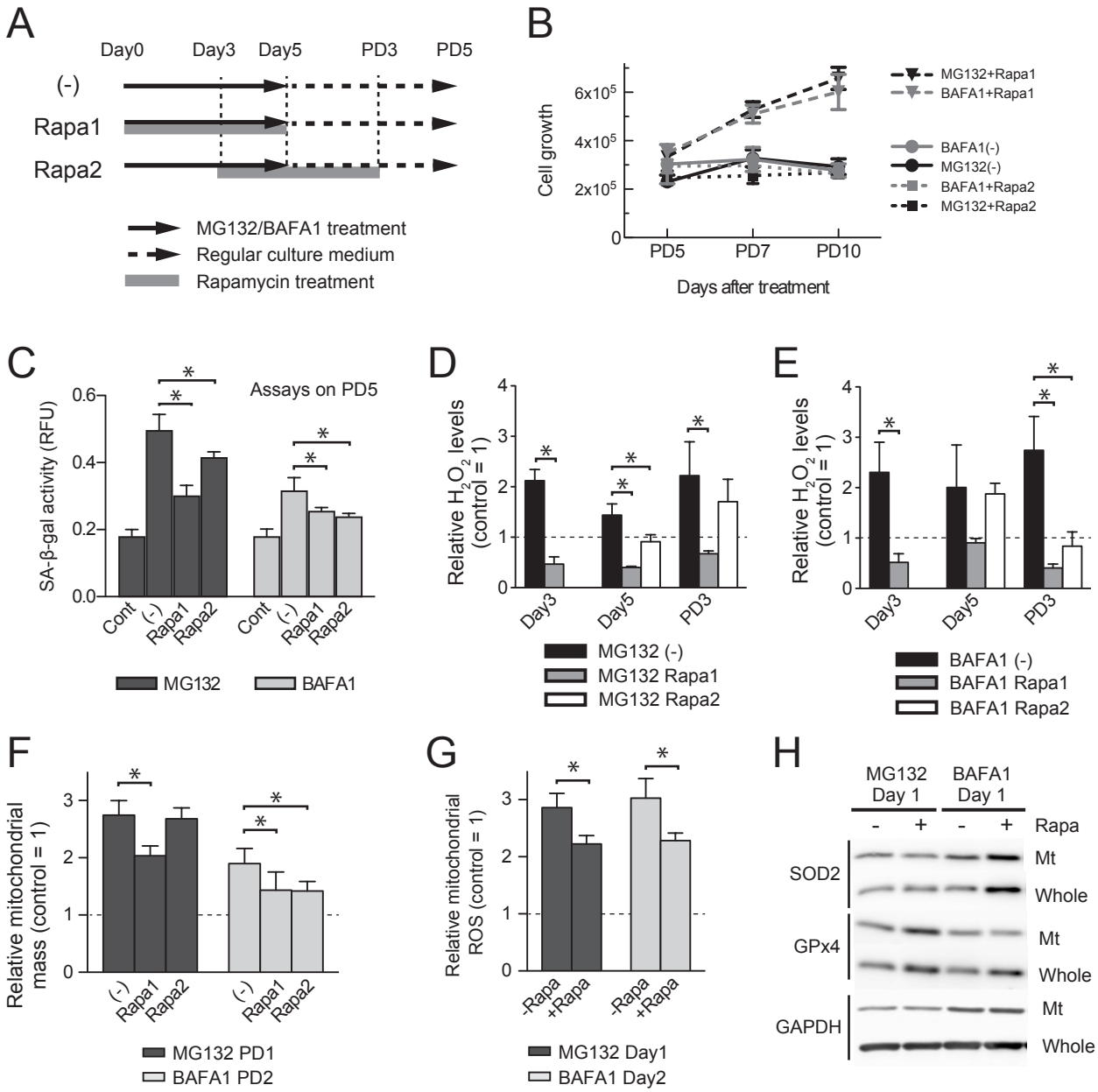
A
Day0
Day3
Day5
PD3
PD5
(-)
Rapa1
Rapa2
MG132/BAFA1 treatment
Regular culture medium
Rapamycin treatment
B
Cell growth
6x10^5
4x10^5
2x10^5
0
PD5
PD7
PD10
Days after treatment
MG132+Rapa1
BAFA1+Rapa1
BAFA1(-)
MG132(-)
BAFA1+Rapa2
MG132+Rapa2
C
SA-β-gal activity (RFU)
Assays on PD5
Cont
(-)
Rapa1
Rapa2
MG132
BAFA1
D
Relative H2O2 levels (control = 1)
Day3
Day5
PD3
MG132 (-)
MG132 Rapa1
MG132 Rapa2
E
Relative H2O2 levels (control = 1)
Day3
Day5
PD3
BAFA1 (-)
BAFA1 Rapa1
BAFA1 Rapa2
F
Relative mitochondrial mass (control = 1)
(-)
Rapa1
Rapa2
MG132 PD1
BAFA1 PD2
G
Relative mitochondrial ROS (control = 1)
-Rapa
+Rapa
MG132 Day1
BAFA1 Day2
H
MG132 Day 1
BAFA1 Day 1
Rapa
SOD2
GPx4
GAPDH
Mt
Whole

Figure 6

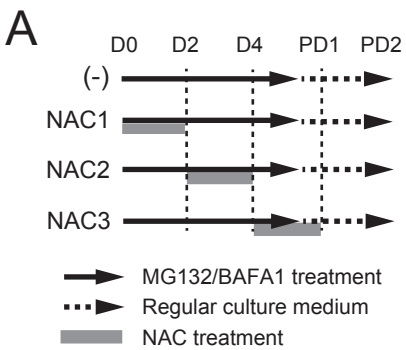
A
D0
D2
D4
PD1
PD2
(-)
NAC1
NAC2
NAC3
MG132/BAFA1 treatment
Regular culture medium
NAC treatment

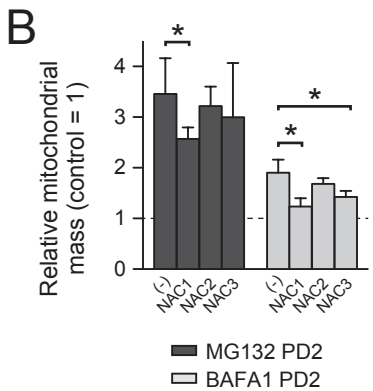
B
Relative mitochondrial mass (control = 1)
0
1
2
3
4
*
*
*
(-)
NAC1
NAC2
NAC3
(-)
NAC1
NAC2
NAC3
MG132 PD2
BAFA1 PD2

Figure 7

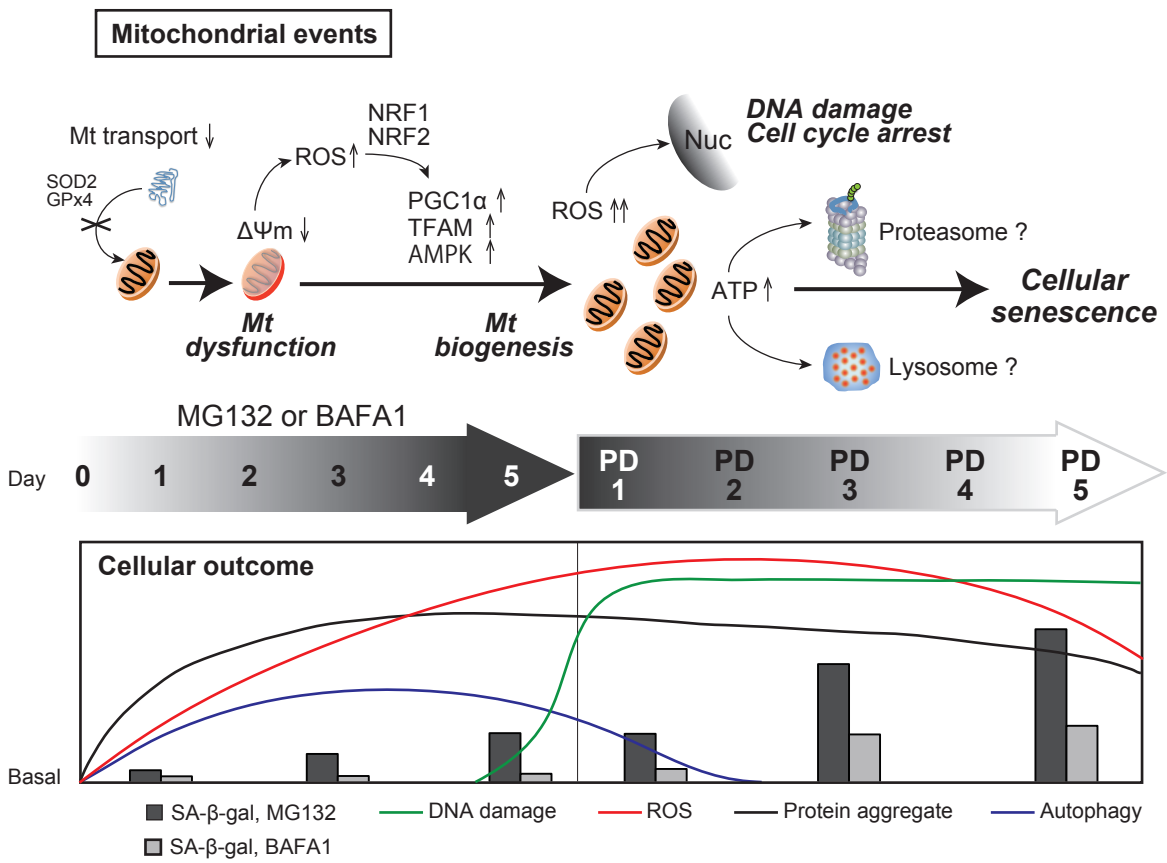
Mitochondrial events
Mt transport ↓
SOD2
GPx4
ΔΨm ↓
ROS ↑
NRF1
NRF2
PGC1α ↑
TFAM ↑
AMPK ↑
Mt dysfunction
Mt biogenesis
ROS ↑↑
Nuc
DNA damage
Cell cycle arrest
ATP ↑
Proteasome ?
Lysosome ?
Cellular senescence
MG132 or BAFA1
Day
0
1
2
3
4
5
PD 1
PD 2
PD 3
PD 4
PD 5
Cellular outcome
Basal
SA-β-gal, MG132
SA-β-gal, BAFA1
DNA damage
ROS
Protein aggregate
Autophagy

Figure S1

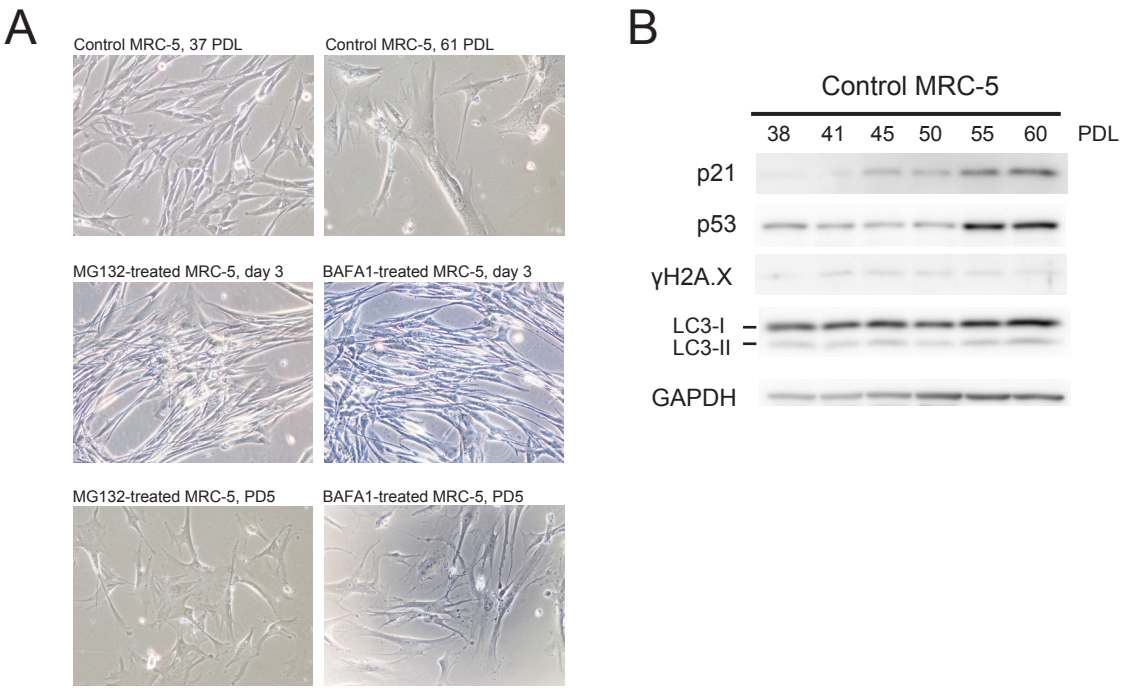

(A) Representative pictures of senescence-induced MRC-5 cells by MG132 or BAFA1 treatment (day 3 and PD5) with young (37 PDL) and aged (61 PDL) control cells.

(B) Immunoblot analysis of untreated control MRC-5 cells undergoing replicative senescence (from 38 to 60 PDL) using antibodies against p21, p53, γH2A.X, LC3,

Figure S2

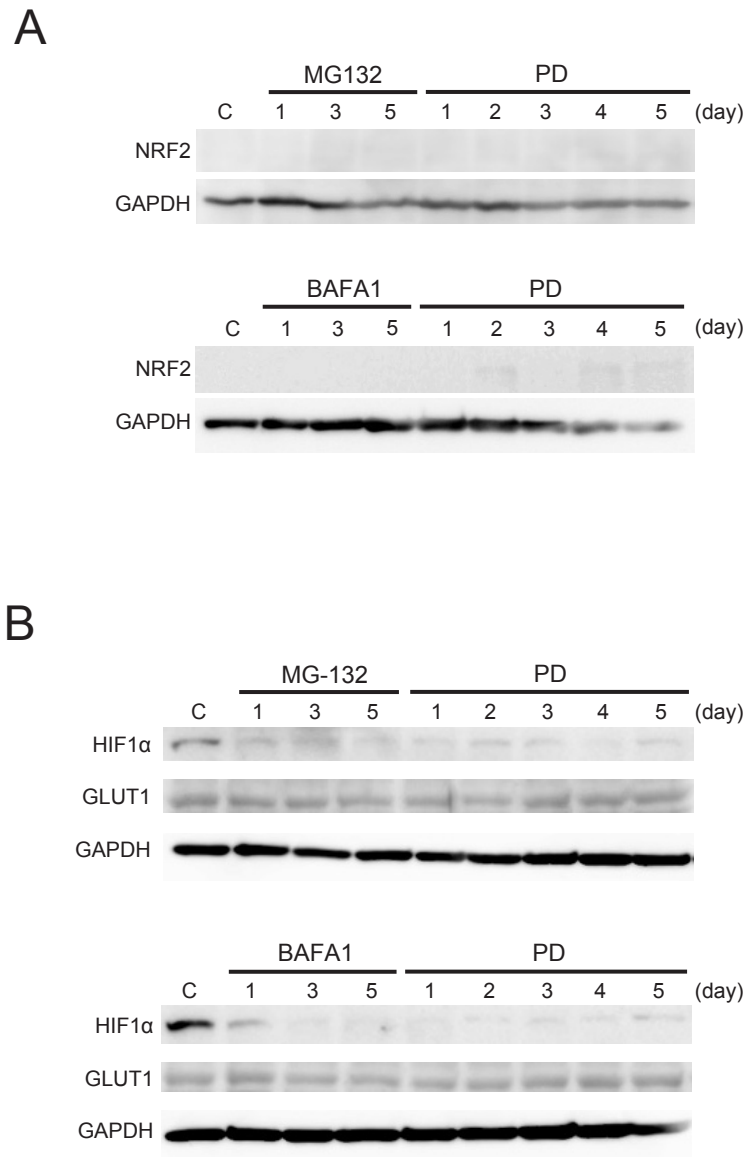

(A) Immunoblot analyses of MG132- or BAFA1-treated cells using antibodies against NRF2 and GAPDH. C, untreated control cells.

(B) Immunoblot analyses of MG132- or BAFA1-treated cells using antibodies against HIF1α, GLUT1, and GAPDH. C, untreated control cells.

Figure S3

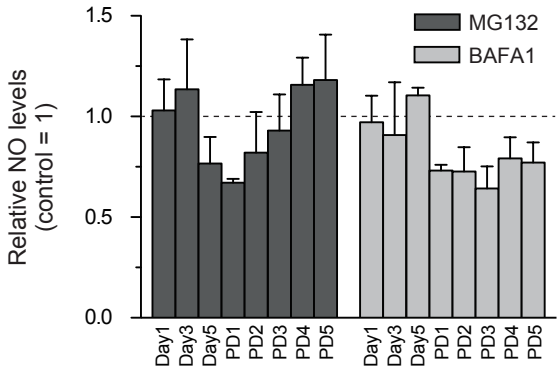

Quantitation of relative intracellular NO levels by using DAF-FM DA fluorescent dye that selectively detects NO. The fluorescence intensity for DAF-FM DA was normalized by total protein concentration. Values are shown as mean ± SD from 4 wells of a 96-well plate.

Figure S4

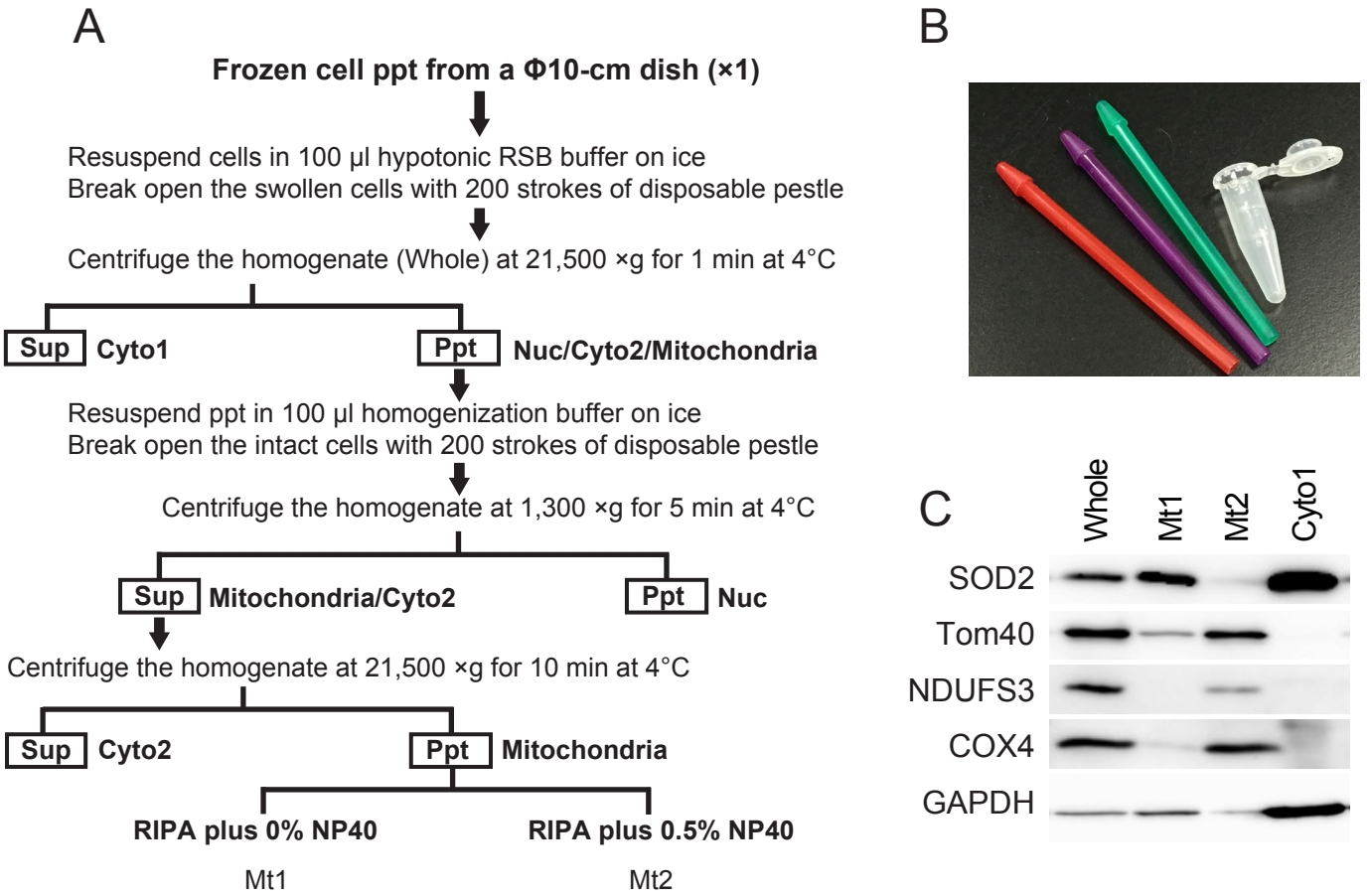

(A) Detailed procedure for preparation of mitochondrial fraction from frozen cell pellet at a microscale. Cells were homogenized in hypotonic RSB buffer, then unbroken cells were repeatedly homogenized in a homogenization buffer. For the immunoblot analyses, solubilized mitochondrial protein in RIPA buffer containing 0.5% NP40 (Mt2) was applied. Hypotonic RSB buffer, 10 mM Tris-HCl, pH7.4, 10 mM NaCl, 1.5 mM $MgCl_2$, protease inhibiter; Homogenization buffer, 5 mM Tris-HCl, pH7.4, 1.5 m$MgCl_2$, 250 mM sucrose, protease inhibitor; RIPA plus 0% NP40, 20 mM Tris-HCl, pH7.4, 50 mM NaCl, 1 mM EDTA, protease inhibitor; RIPA plus 0.5% NP40, 20 mM Tris-HCl, pH7.4, 50 mM NaCl, 0.5% Nonidet P-40, 0.05% SDS, 1 mM EDTA, protease inhibitor; Cyto, cytoplasmic fraction; Nuc, nuclear fraction; Whole, whole cellular extract. (B) Disposable plastic pestles and a matched Safe-Lock tube used in this method. (C) Immunoblot analyses of whole cellular extract (Whole), mitochondrial fractions 1 and 2 (Mt1 and 2), and cytoplasmic fraction (Cyto1) prepared from untreated control MRC5 cells using antibodies against SOD2, Tom40, NDUFS3, COX4, and GAPDH.

Figure S5

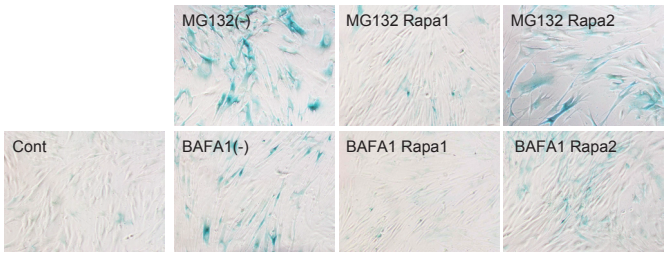

Representative pictures of SA-β-gal positive MRC-5 cells. Cells were co-treated with rapamycin and either MG132 or BAFA1 for 5 days, respectively, and stained at PD5 (cytoplasmic blue precipitate). Control, untreated young (39 PDL) MRC-5 cells. (-), cells treated with only MG132 or BAFA1; Rapa1 and Rapa2, cells co-treated with rapamycin and either MG132 or BAFA1 as shown in Fig. 5A.

Figure S6

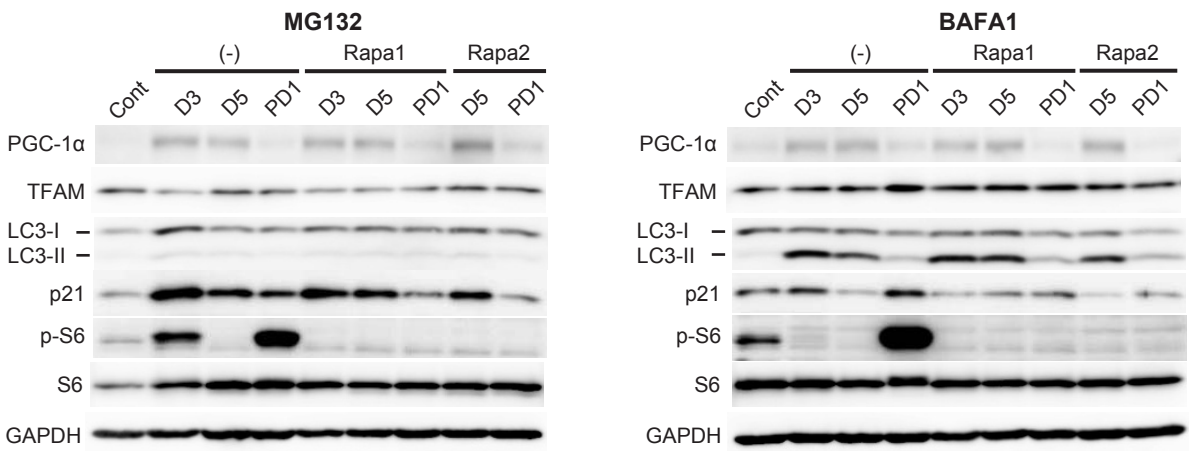

Immunoblot analyses of MG132 (left)- or BAFA1 (right)-treated cells with (Rapa1 and Rapa2) or without (-) rapamycin at day 3 (D3), day 5 (D5), and PD1.